J Therm Spray Tech (2019) 28:1060–1071
https://doi.org/10.1007/s11666-019-00869-x

PEER REVIEWED

A Comparative Study of Cavitation Erosion Resistance of Several HVOF-Sprayed Coatings in Deionized Water and Artificial Seawater

Haijun Zhang[1] · Yongfeng Gong[1] · Xiuyong Chen[1,2,3] · André McDonald[3] · Hua Li[1,2]

Submitted: 30 December 2018 / in revised form: 29 April 2019 / Published online: 13 May 2019

Abstract In this study, WC-10Co4Cr coatings, Co-based coatings, WC-10Co4Cr/Co-based composite coatings, and Fe-based amorphous/nanocrystalline coatings were prepared on 316L stainless steel substrates by a high-velocity oxy-fuel spraying process. The cavitation erosion resistances of all the coatings, as well as the stainless steel substrates, were investigated in deionized water and artificial seawater. Results show that the effect of marine corrosion on cavitation erosion was most significant on the stainless steels, WC-10Co4Cr coatings, and Co-based coatings, but negligible on the WC-10Co4Cr/Co-based composite coatings and the Fe-based amorphous/nanocrystalline coatings. The WC-10Co4Cr coatings (0.17 mm^3/h) show improved cavitation erosion resistance than those of WC-10Co4Cr/Co-based composite coatings (0.21 mm^3/h), 316L stainless steel substrates (0.22 mm^3/h), Co-based coatings (0.30 mm^3/h), and Fe-based coatings (0.47 mm^3/h) in marine environments.

Haijun Zhang and Yongfeng Gong have contributed equally to this work.

✉ Xiuyong Chen
chenxiuyong@nimte.ac.cn

✉ Hua Li
lihua@nimte.ac.cn

[1] Key Laboratory of Marine Materials and Related Technologies, Zhejiang Key Laboratory of Marine Materials and Protective Technologies, Ningbo Institute of Materials Technology and Engineering, Chinese Academy of Sciences, Ningbo 315201, China

[2] Cixi Institute of Biomedical Engineering, Ningbo Institute of Materials Technology and Engineering, Chinese Academy of Sciences, Ningbo 315201, China

[3] Department of Mechanical Engineering, University of Alberta, Edmonton, AB T6G 1H9, Canada

Keywords cavitation erosion · coatings · HVOF · marine corrosion

Introduction

Cavitation is a surface degradation process in which vapor bubbles in a low-pressure liquid form and collapse, usually explosively, at surfaces and within the liquid causing severe surface erosion and material removal or vibrations of the devices in which the liquid is enclosed. Cavitation erosion commonly causes damage in hydrodynamic systems, shortening their service life, reducing their operating efficiency, and increasing cost (Ref 1, 2). In addition, chlorine ions in seawater can cause electrochemical corrosion, resulting in a synergistic effect with the cavitation damage (Ref 3, 4). Generally, two strategies are used to reduce cavitation erosion damage: optimal design of hydrodynamic profiles and development of novel alloys/coatings to provide enhanced cavitation erosion protection (Ref 5). Surface treatment techniques, such as twin-wire arc spraying (Ref 6), plasma spraying or plasma-transferred arc welding (Ref 7), laser surface alloying (Ref 8-10), and high-velocity oxy-fuel (HVOF) spraying (Ref 11), have been widely used to deposit erosion-resistant coatings. Among various techniques, HVOF spraying has been widely employed to prepare coatings with higher hardness, reduced decarburization, lower porosity, and higher bond strength (Ref 12).

To date, many kinds of coating materials such as ceramics (Ref 13, 14), engineering alloys (Ref 15), and plastics (Ref 16) have been tested on metal alloy components to combat cavitation erosion, with some success. For example, cobalt-based Stellite alloy coatings prepared by HVOF spraying have been used as hardfacing materials due to their resistance

to cavitation and corrosion (Ref 17, 18). HVOF-sprayed Fe-based amorphous/nanocrystalline coatings and tungsten carbide (WC)-based coatings have been widely reported to improve cavitation erosion resistance in hydrodynamic systems (Ref 19-22), with WC-based coatings generally receptive as wear-resistant material coatings for aggressive wear environments (Ref 23-25). However, the cavitation erosion mechanism of coatings in corrosive seawater remains unclear. It has been reported that, due to the synergistic effects of cavitation erosion and corrosion in an environment as harsh as seawater and 3.5% NaCl solution, erosion increases compared with the result in deionized water (Ref 26). It has been shown by further by Neville et al. (Ref 23) that the dissolution of WC in metal matrix composite coatings (MMC) during fabrication with high-temperature deposition processes such as plasma-transferred arc welding results in the formation of intermetallic phases with the binder alloys in the MMC, which form micro-galvanic cells to undermine the corrosion resistance, and ultimately, the erosion resistance, of the overlay coating. It is worth noting, however, that results are contrary to those discovered by Hong et al. (Ref 5) who found that WC-17Co cermet coating, TC4 titanium alloy, NiCr alloy coating, and WC-17Co/NiCr composite coating possessed better cavitation erosion resistance in artificial seawater than that in deionized water. Thus, ongoing efforts are still needed to elucidate the true effect of corrosion on the cavitation behavior of HVOF-sprayed coatings used for marine applications in corrosive environments.

In the present study, WC-10Co4Cr coatings, Co-based coatings, WC-10Co4Cr/Co-based composite coatings, and Fe-based amorphous/nanocrystalline coatings were prepared by utilizing high-velocity oxy-fuel (HVOF) spraying. The cavitation erosion properties of the coatings, as well as those of control 316L stainless steel substrates, were evaluated in deionized water and artificial seawater. The coatings prepared by HVOF spraying here might show a potential application as cavitation resistance coatings for ship propellers.

Materials and Experimental Methods

Materials and Coating Preparation

The substrates used in this study were 316L stainless steel (316L SS, C $\leq$ 0.03%, Si $\leq$ 1.00%, Mn $\leq$ 2.00%, P $\leq$ 0.035%, S $\leq$ 0.03%, Ni: 10.0-14.0%, Cr: 16.0-18.0%, Mo: 2.0-3.0%) plates with dimensions of 20 $\times$ 10 $\times$ 2 mm. Commercially available WC-10Co4Cr powders (Oerlikon Metco Surface Technology (Shanghai) Co. Ltd, China) and Co-based powders ($Co_{62.44}Cr_{27.32}Ni_{3.01}Si_{1.33}Mo_{5.9}$, Shanghai Global Fusion Materials Technology Co. Ltd, China) were used in this study. The iron-based powders ($Fe_{53}Cr_{19}Zr_7Mo_2C_{18}Si$, 30 to 150 μm) were obtained from the University of Science and Technology Beijing, China. Four types of coatings were deposited on the 316L SS substrates by using a high-velocity oxy-fuel (HVOF) spray torch (CJK5, Castolin Eutectic, Germany) using kerosene and oxygen as the gases, respectively. Nitrogen was used as the carrier gas for the powder. Different powder feed rates were used for the powders, and the spraying distance or standoff distance was 300 mm. The details of the spray parameters used in this study are given in Table 1. Artificial seawater (ASW) was prepared in accordance with the requirements of ASTM Standard D1141-98 (2003) (Ref 27).

Characterization of Coatings

The microstructure of the powders and the coatings was characterized by using field emission scanning electron microscopy (FESEM, FEI Quanta FEG250, Netherlands), with energy-dispersive spectroscopy (EDS, X-max, Oxford Instrument Technology Co., Ltd, England). The SEM images of the coatings (cross-sectional view) were analyzed using Adobe Photoshop CS6 to calculate their porosities. Three measurements were taken in this study. The phase composition of the coatings was examined by using x-ray diffraction (XRD, D8 Advance, Bruker AXS, Germany). The amorphicity of the Fe-based coating was calculated according to the equation: $X_a = 1 - \frac{I_c}{I_c+I_a} \times 100\%$, where X_a is the amorphicity, I_a is the amorphous scattering intensity, and I_c is the crystal diffraction intensity. A copper anode was used at 40 kV and 40 mA, and a monochromator was used to filter *K*-beta wavelengths. Continuous XRD mode, where the 2θ diffraction angle was changed from 20° to 90° at a step size of 0.033°, was used.

Cavitation Erosion Testing of the Coatings

Cavitation erosion tests were performed using vibratory cavitation equipment (GBS-SCT 20A, Guobiao Ultrasonic Equipment Co., Ltd., Hangzhou, China) as a simplified controllable test, in accordance with ASTM Standard G32-16, to investigate fluid cavitation, for example, in ship propellers (Ref 28). The cavitation mechanisms in this method and those that generated during operation of ship propellers are different, but the nature of the material failure mechanism is thought to be similar (Ref 28). Prior to cavitation erosion testing, the coatings were polished to a mirror finish, cleaned with acetone, dried in warm air, and finally weighed using an analytical balance (Mettler 220, Toledo Instruments Co., Ltd., Shanghai, China) with an accuracy of 0.1 mg. The schematic of the cavitation erosion test apparatus is shown in Fig. 1. The double

Table 1 Parameters for HVOF spraying

Spray parameters	Coating			
	WC-10Co4Cr	Co-based	Composite	Fe-based
Oxygen flow, mL/min	845	800	800	800
Kerosene flow, mL/min	480	400	400	400
Spraying distance, mm	300	300	300	300
Carrier gas flow, mL/min	9.9	8.5	8.5	8.5
Powders feed rate, g/min	11.9	15.3	15.3	35

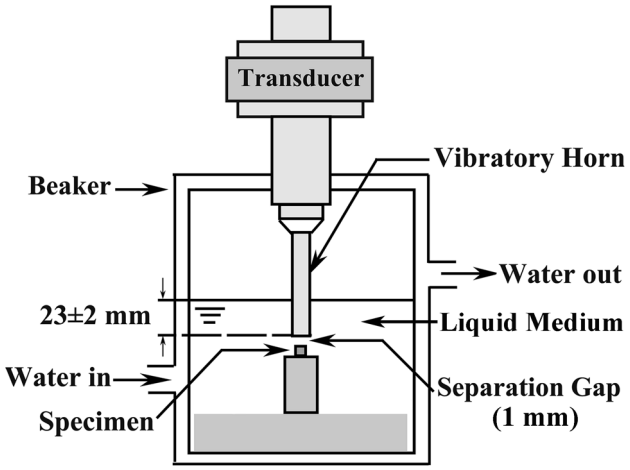

Fig. 1 Schematic diagram of the cavitation erosion test system

amplitude and the vibration frequency used in this study were 50 μm and 20 kHz, respectively. The test liquids were distilled water and ASW, which were maintained at 25 ± 2 °C. The oscillating horn was immersed in the test liquid to a depth of 23 ± 2 mm. The samples were fixed below the vibrating horn at a distance of 1 mm (Ref 22). The cavitation tests were performed for 15 h at intervals of 1 h, and the mass loss of the samples was recorded after each hour of testing. The volume loss was gained by means of dividing mass loss by density, and then, the rate of volume loss was obtained through dividing volume loss by time. The volume loss and rate of volume loss were estimated for three samples of the same type in order to confirm reproducibility and allow for statistical analyses. After the tests, the morphologies of the eroded scars of the tested coatings were analyzed by using images captured through FESEM.

Results and Discussion

Structure of the Powders and the Coatings

Scanning electron microscope images of the WC-10Co4Cr powders, Co-based powders, WC-10Co4Cr/Co-based composite powders (1:1), and the Fe-based powders are shown in Fig. 2. It can be seen that both the gas-atomized WC-10Co4Cr powders (15 to 45 μm) and the Co-based powders (10 to 40 μm) are nearly spherical (Fig. 2a and b). The WC-10Co4Cr/Co-based composite powders were prepared by mixing the WC-10Co4Cr powder and Co-based powder in a 1:1 ratio (Fig. 2c). The gas-atomized Fe-based powders (30 to 150 μm) were also nearly spherical, which are suitable for HVOF spraying (Fig. 2d).

The x-ray diffraction patterns of the powders and the as-sprayed coatings are shown in Fig. 3. The WC-10Co4Cr powders were mainly composed of WC, Co, and Co_3W_3C phases, and the coating was mainly composed of WC phase (Fig. 3a). The phases of W_2C and W_6Co_6C were absent in the feedstock powders, but were present in the as-sprayed coating. This is because WC particles were partially decarburized and dissolved in the cobalt matrix during the spray process (Ref 29). The major phases in the Co-based powders and coating consisted of Co, Cr_2Ni_3, and $Cr_{5.04}Mo_{11.76}Ni_{11.2}$ phases (Fig. 3b) and the composite coating was mainly comprised of WC, $Cr_{17.4}Co_{29}Si_{11.6}$, and Mo_2C phases (Fig. 3c), which indicated that metallurgical reactions were present between the two kinds of powders during the thermal spraying process. This can be due to the metallurgical reactions, which usually manifest in coatings by the formation of intermetallics of the constituent material phases. As the diffraction pattern in Fig. 3(d) shows, Fe-based coatings with hybrid amorphous/nanocrystalline structures were obtained. The intensity of the crystalline peak was much lower than that of the as-received powders, indicating that amorphicity of the HVOF-deposited coating increased to approximately 47.3%. Further, the primary crystalline phase was α-Fe (from JCPDS Card No.: 65-4899). These results are similar to those that were obtained from recent studies (Ref 30, 31).

Figure 4 presents SEM images of the cross sections of the coatings that were studied. Coatings with a thickness of approximately 200 μm were successfully fabricated with limited three-dimensional defects such as pores. The average porosities of the WC-10Co4Cr coating, the Co-based coating, the WC-10Co4Cr/Co-based composite coating, and Fe-based amorphous/nanocrystalline coating

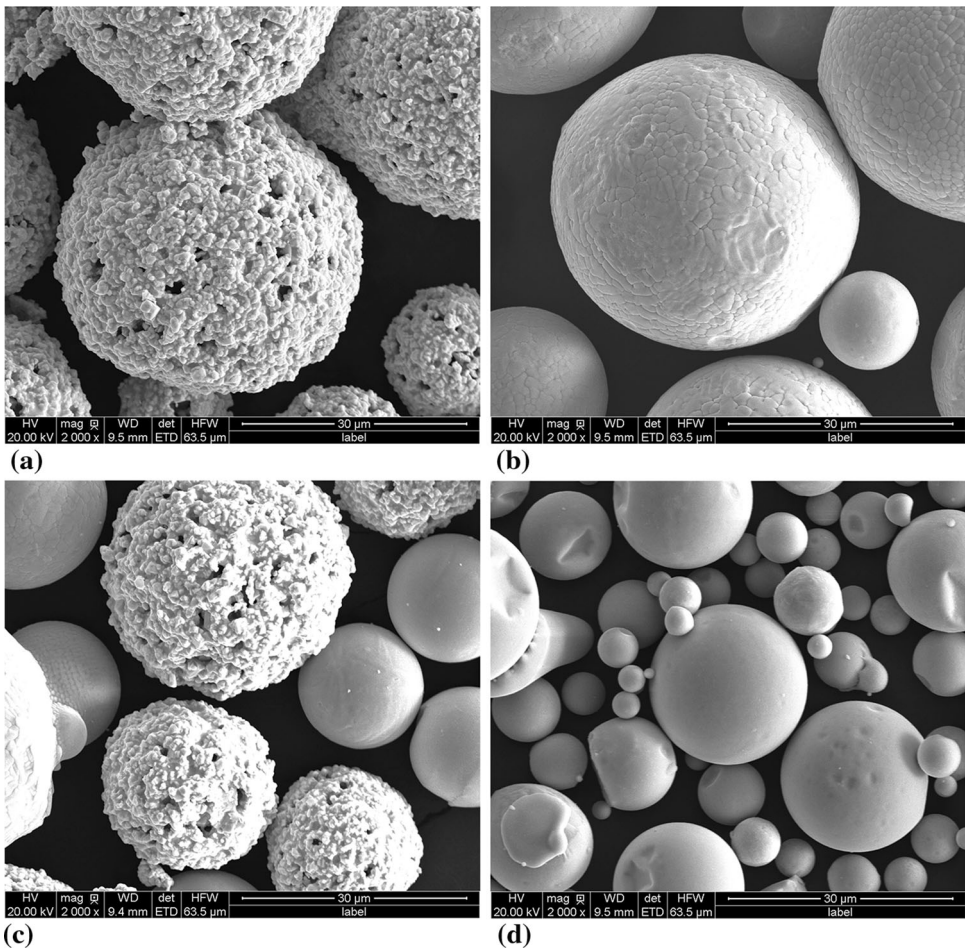

Fig. 2 FESEM images of (a) WC-10Co4Cr powders, (b) Co-based powders, (c) WC-10Co4Cr/Co-based composite powders, and (d) Fe-based powders

were approximately 2.3, 0.6, 2.0, and 2.7%, respectively (Table 2). Partially melted particles can be observed in the Co-based coating indicated by arrows in Fig. 4(b). Pronounced particle boundaries are evident, which likely led to reduced cohesion in the Co-based coating. The WC-10Co4Cr/Co-based composite coating showed uniform distribution of the WC-10Co4Cr (indicated by black arrows in Fig. 4c) and $Cr_{17.4}Co_{29}Si_{11.6}$ phases (indicated by red arrows in Fig. 4c). The Fe-based amorphous/nanocrystalline coating shows a lamellar microstructure (Fig. 4d).

Cavitation Erosion and Corrosion of the Coatings

Figure 5 shows the relationship between the volume loss rate of the coatings and the cavitation erosion time in deionized water (Fig. 5a) and in artificial seawater (Fig. 5b). The cumulative volume loss rates of the WC-10Co4Cr coating tested in deionized water were significantly lower than those of the other three kinds of coatings (see Fig. 5a). With the increase in cavitation erosion time, the cavitation erosion rates of the coatings gradually declined and ultimately stabilized. After 15 h of cavitation erosion testing, the cumulative volume loss rates of the five types of coatings were as follows: WC-10Co4Cr coating (0.06 mm^3/h) < 316L stainless steel substrate (0.09 mm^3/h) < Co-based coating (0.11 mm^3/h) < WC-10Co4Cr/Co-based composite coating (0.30 mm^3/h) < Fe-based coating (0.58 mm^3/h). It is worth noting that, with the exception of the WC-10Co4Cr coating, the rates of volume loss for all the other coatings were higher than that of the 316L stainless steel substrate. This may be because the surface porosity of the coatings serves as prefabricated cavitation pits and becomes preferential cavitation initiation sites (Ref 32). Though all the coatings were polished to a mirror finish with the same surface roughness before the cavitation erosion tests were conducted, porosity present in the coating is known to increase the volume loss rate at the beginning of the cavitation erosion test (Ref 26). It is also generally known that materials with higher hardness possess better cavitation erosion resistance (Ref 33). Although the combination of amorphous and nanocrystalline phases gave rise to high hardness for the Fe-based coating (Ref 34) (see Table 2), due to its elevated porosity of approximately 2.7% (see Table 2), it also showed the lowest resistance to cavitation erosion. Further, pronounced particle boundaries in the coating (see Fig. 4b and d) may lead to reduced

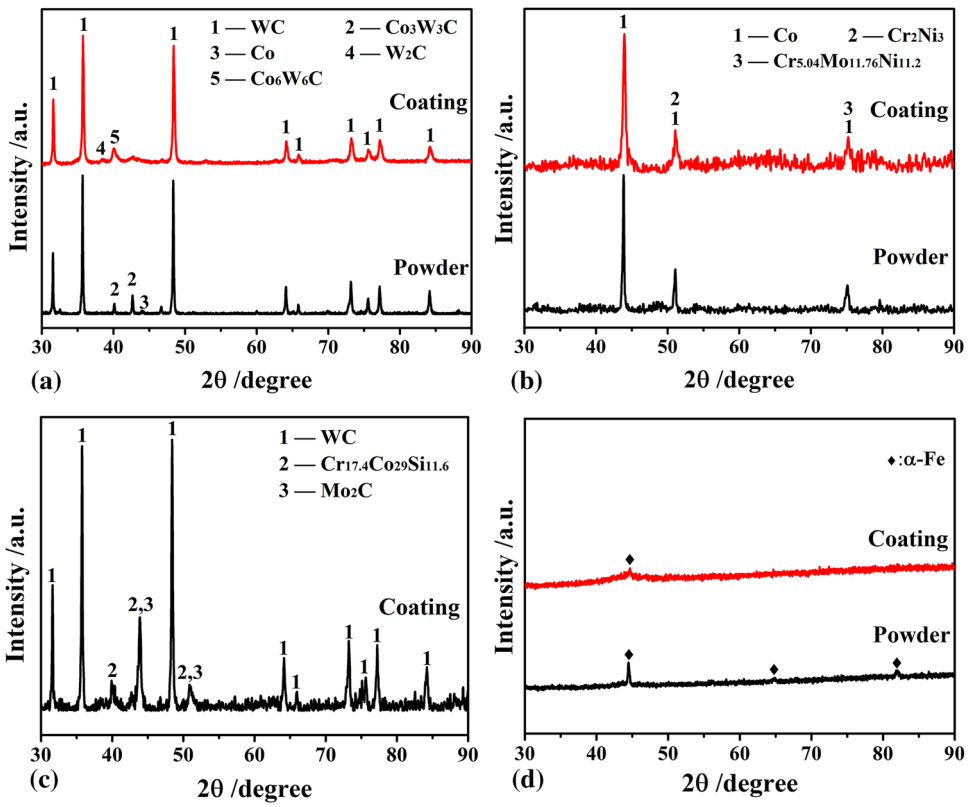

Fig. 3 XRD patterns of the powders and coatings: (a) WC-10Co4Cr, (b) Co-based, (c) WC-10Co4Cr/Co-based composite, and (d) Fe-based

cohesion of the coating because of the partial melting of the powder particles during deposition and cavitation erosion cracks may preferentially grow along particle boundaries where there is poor contact within the coating itself, thus resulting in severe cavitation erosion material loss.

Corrosion is known to have an adverse impact on materials during cavitation, and cavitation erosion processes are much more complex in seawater (Ref 26, 35, 36). Therefore, tests were also conducted in artificial seawater, and the erosion results are shown in Fig. 5(b). The following ranking of cumulative volume loss rates of the coatings tested in artificial seawater after 15 h of exposure was established: WC-10Co4Cr coating (0.17 mm^3/h) < WC-10Co4Cr/Co-based composite coating (0.21 mm^3/h) < 316L stainless steel substrate (0.22 mm^3/h) < Co-based coating (0.30 mm^3/h) < Fe-based coating (0.47 mm^3/h). The ranking is similar to the one for the tests that were conducted in deionized water, except that the position of the WC-10Co4Cr/Co-based composite coating and the 316L stainless steel substrate has changed. Nevertheless, during the first 12 h of cavitation erosion testing, the volume losses in all four types of as-sprayed coatings were higher than those in the 316L stainless steel. Thus, taken together, the results show that the WC-10Co4Cr coating exhibits the best cavitation erosion resistance in both deionized water and artificial seawater, as compared to the other three coating samples and the uncoated substrates.

It is generally reported that mechanical cavitation and electrochemical corrosion coexist when cavitation takes place in corrosive media, and together, they may accelerate the rate of volume loss and the deterioration of the materials (Ref 37). To evaluate the effect of marine corrosion on the cavitation process over a variety of different materials, a comparative study of cavitation erosion resistance in deionized water and artificial seawater was conducted, as shown in Fig. 6, which shows the relationship between the cumulative volume loss of the coatings and cavitation erosion time in both liquid media. The cumulative volume losses of the 316L stainless steel in deionized water and in artificial seawater were 1.33 and 3.37 mm^3, respectively (see Fig. 6a). A similar trend was observed for the WC-10Co4Cr coating and Co-based coating (Fig. 6b and c). After cavitation erosion for 15 h, the cumulative volume losses of the WC-10Co4Cr coating and Co-based coating in artificial seawater were 2.56 and 4.53 mm^3, respectively, which are approximately three times those of the coatings that were tested in deionized water. This phenomenon occurred because the cavitation resistance of these materials was significantly reduced due to their inferior corrosion resistance in an environment in which chloride ions (Cl^-) were present (Ref 26, 38, 39). Pores, cracks, and

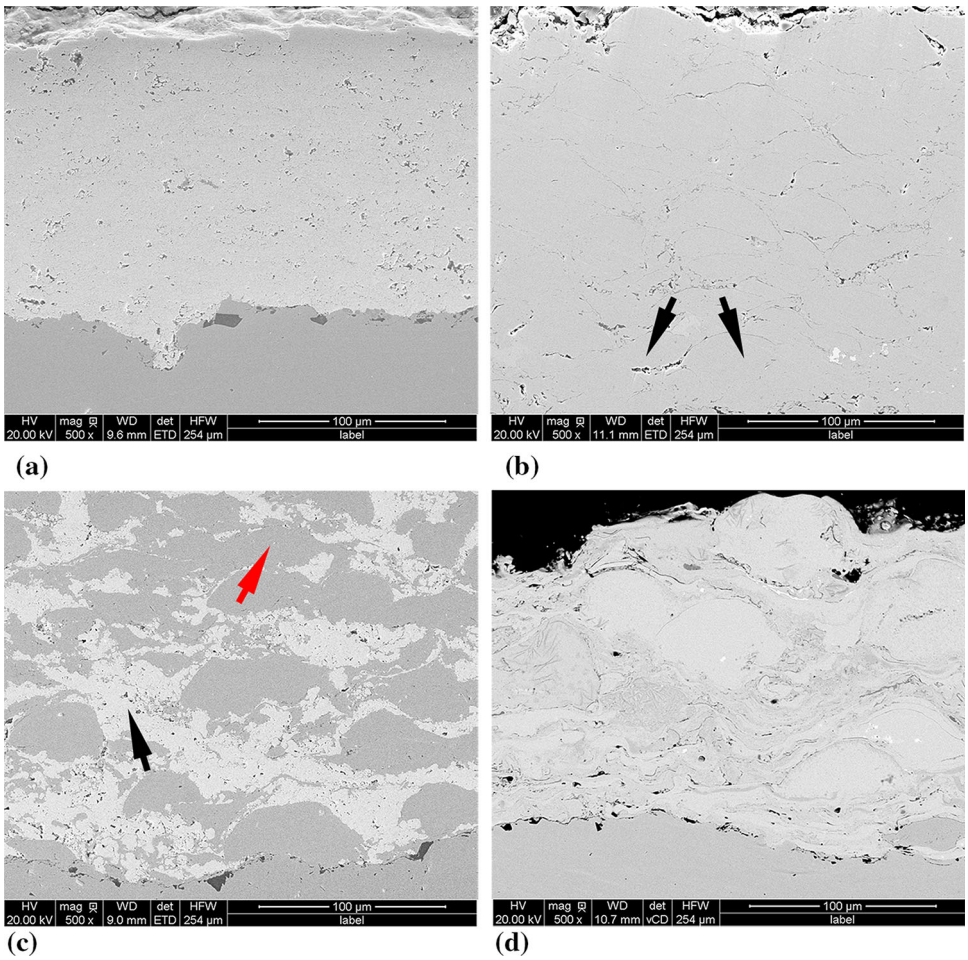

Fig. 4 FESEM images of the cross-sectional morphologies of (a) WC-10Co4Cr coating, (b) Co-based coating (black arrows indicate partially melted particles), (c) WC-10Co4Cr/Co-based composite coating (black arrow indicates WC-10Co4Cr phase; red arrow indicates $Cr_{17.4}Co_{29}Si_{11.6}$ phase), and (d) Fe-based coating

Table 2 Hardness and porosities of the HVOF-sprayed coatings and the 316L stainless steel substrates

Samples	Hardness ($HV_{0.3}$) (n = 3)	Porosity, % (n = 3)
316L stainless steel	163.89 ± 3.8	…
WC-10Co4Cr coating	1273.1 ± 182.7	2.3 ± 0.05
Co-based coating	617.7 ± 46.1	0.6 ± 0.08
WC-10Co4Cr/Co-based composite coating	757.1 ± 109.6	2.0 ± 0.07
Fe-based coating	959.2 ± 92.4	2.7 ± 0.10

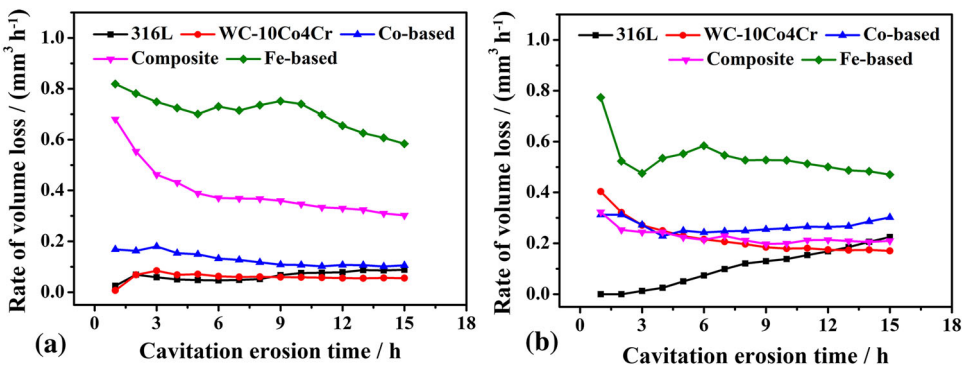

Fig. 5 Rates of volume loss of 316L stainless steel, WC-10Co4Cr coating, Co-based coating, WC-10Co4Cr/Co-based composite coating, and Fe-based coating after cavitation exposure of 15 h in deionized water (a) and in artificial seawater (b)

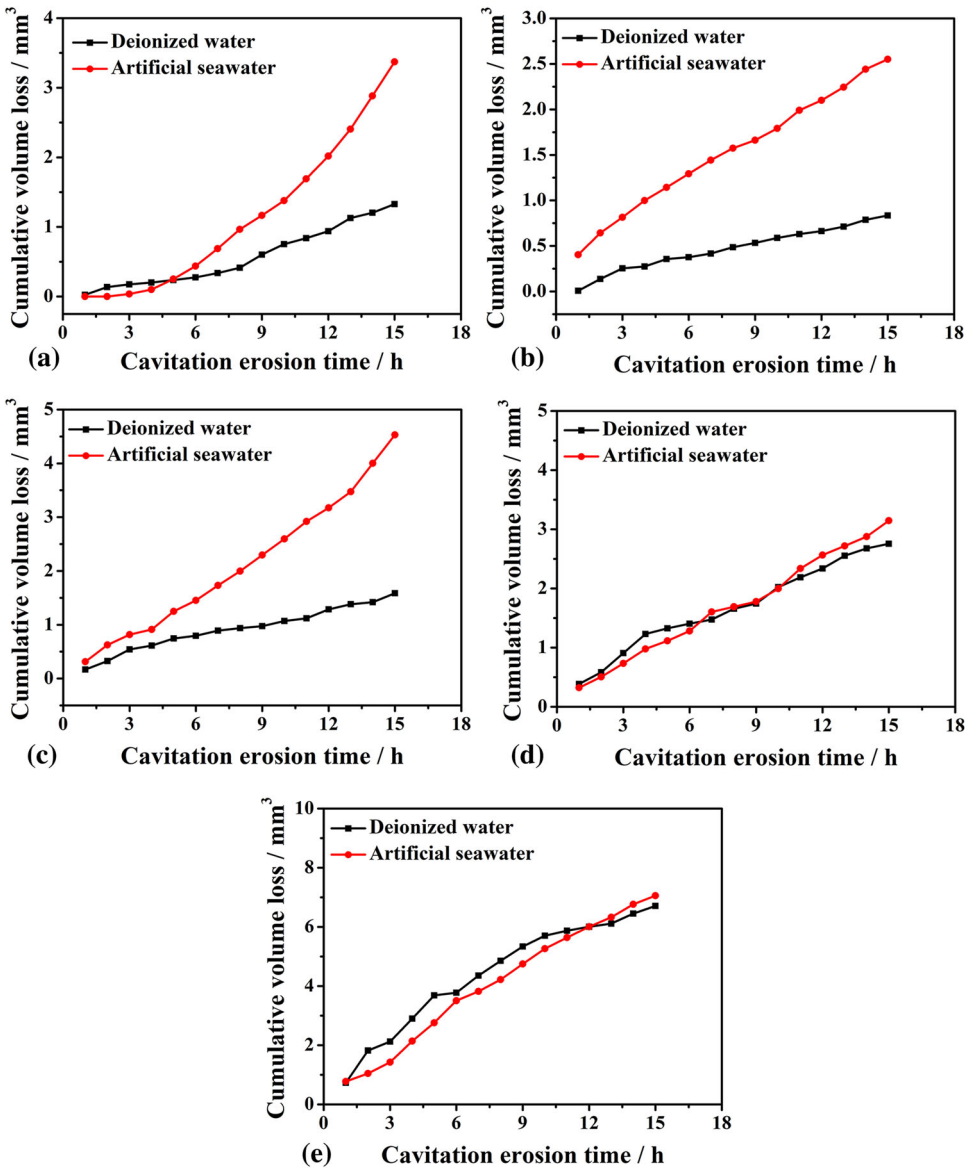

Fig. 6 Effect of marine corrosion on the cavitation resistance of investigated specimens tested in deionized water and artificial seawater. (a) 316L stainless steel, (b) WC-10Co4Cr coating, (c) Co-based coating, (d) WC-10Co4Cr/Co-based composite coating, and (e) Fe-based coating

interlamellar boundaries are regarded as preferred locations for corrosion nucleation and growth (Ref 40). However, the cumulative volume losses of the WC-10Co4Cr/Co-based composite coating and Fe-based coating in deionized water were 2.76 and 6.71 mm^3, respectively, and showed only a slight increase to 3.14 and 7.05 mm^3, respectively, in artificial seawater (Fig. 6d and e). The synergistic effect of cavitation erosion and marine corrosion became dominant for the 316L stainless steel, WC-10Co4Cr coating, and Co-based coating. On the other hand, mechanical cavitation was the main cause of cavitation erosion–corrosion degradation in the WC-10Co4Cr/Co-based composite and Fe-based coating materials. This result was similar to that of a previous study by Hong et al. (Ref 26). However, the WC-10Co4Cr coating showed a higher cavitation erosion resistance in deionized water rather than in artificial seawater, which is contrary to an existing report (Ref 5). This is likely due to their inferior corrosion resistance (Ref 1), lower fracture toughness (Ref 41), and the existence of unmelted particles in the coating (Ref 42). Due to the chloride ions in the artificial seawater and the stress caused by bubble collapse at the coating surface during cavitation, further extension of cracks may directly lead to interlamellar cohesive detachment within the coating, exfoliation of WC particles, and the formation of large cavitation craters on the surface of the coating. Cohesive delamination and damage are also more likely because the products of corrosion were non-adherent and hence did not provide sufficient protection during the cavitation erosion tests in the corrosive environment (Ref 4).

Surface Damages after Cavitation Erosion

SEM was performed to capture images of the detailed cavitation/cavitation–corrosion damage of the specimens before (Fig. 7) and after 15 h of cavitation erosion testing in deionized water (Fig. 8) and in artificial seawater (Fig. 9). Before the cavitation test, no obvious pits could be detected on the polished 316L stainless steel surface (Fig. 7a); however, evidence of pits was observed on the surface of the WC-10Co4Cr coating (Fig. 7b). For the Co-based coating, significant pits were observed (Fig. 7c). Moreover, the pits on the WC-10Co4Cr/Co-based composite coating with uniform distribution of WC-10Co4Cr and Co-based phases were more noticeable than those on the Co-based coating (compare Fig. 7c and 7d). However, for the Fe-based coating, more defects were observed as

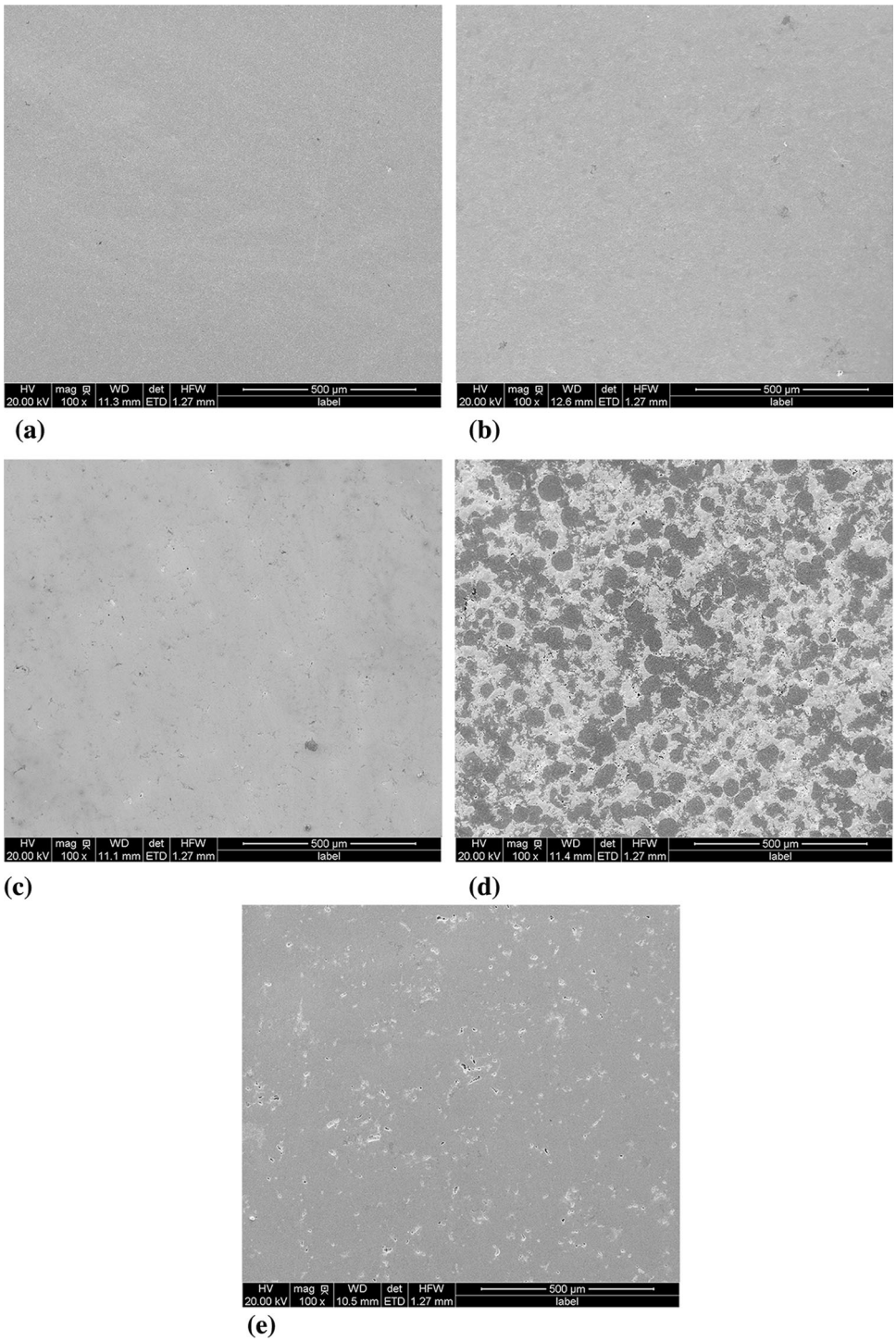

Fig. 7 FESEM morphologies of the surfaces of (a) 316L stainless steel, (b) WC-10Co4Cr coating, (c) Co-based coating, (d) WC-10Co4Cr/Co-based composite coating, and (e) Fe-based coating before cavitation test

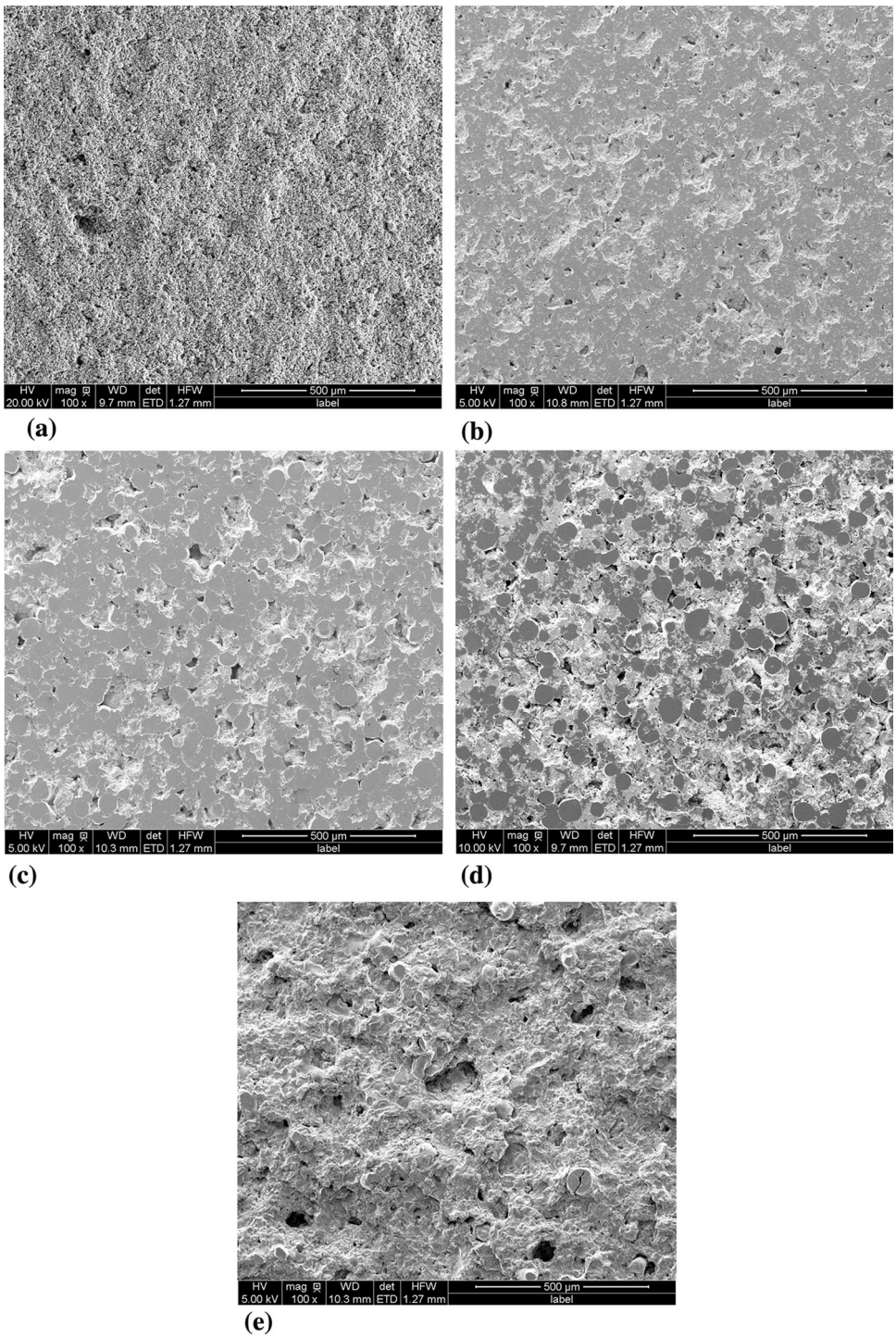

Fig. 8 FESEM morphologies of the surfaces of (a) 316L stainless steel, (b) WC-10Co4Cr coating, (c) Co-based coating, (d) WC-10Co4Cr/Co-based composite coating, and (e) Fe-based coating after cavitation exposure of 15 h in deionized water

indicated by the numerous pits (Fig. 7e). This result is consistent with the porosity data (Table 2). After cavitation test, it was clearly observed that some smaller cavitation pinholes and cavitation erosion craters were present on the eroded surface of the 316L stainless steel (Fig. 8a). The cavitation-damaged surface for the WC-10Co4Cr coating also indicated the distribution of pinholes and some micropores and micro-cracks at the bottom of the cavitation craters (Fig. 8b). The pores on the surface of the WC-10Co4Cr coating were likely the result of cavitation erosion pits. For the Co-based coating (Fig. 8c), upon examination of the damaged surfaces it was determined that material removal was mainly due to the presence of cavitation cracks and then the detachment of large particles because of weak bonding between unmelted particles. For the WC-10Co4Cr/Co-based composite coating, the surface

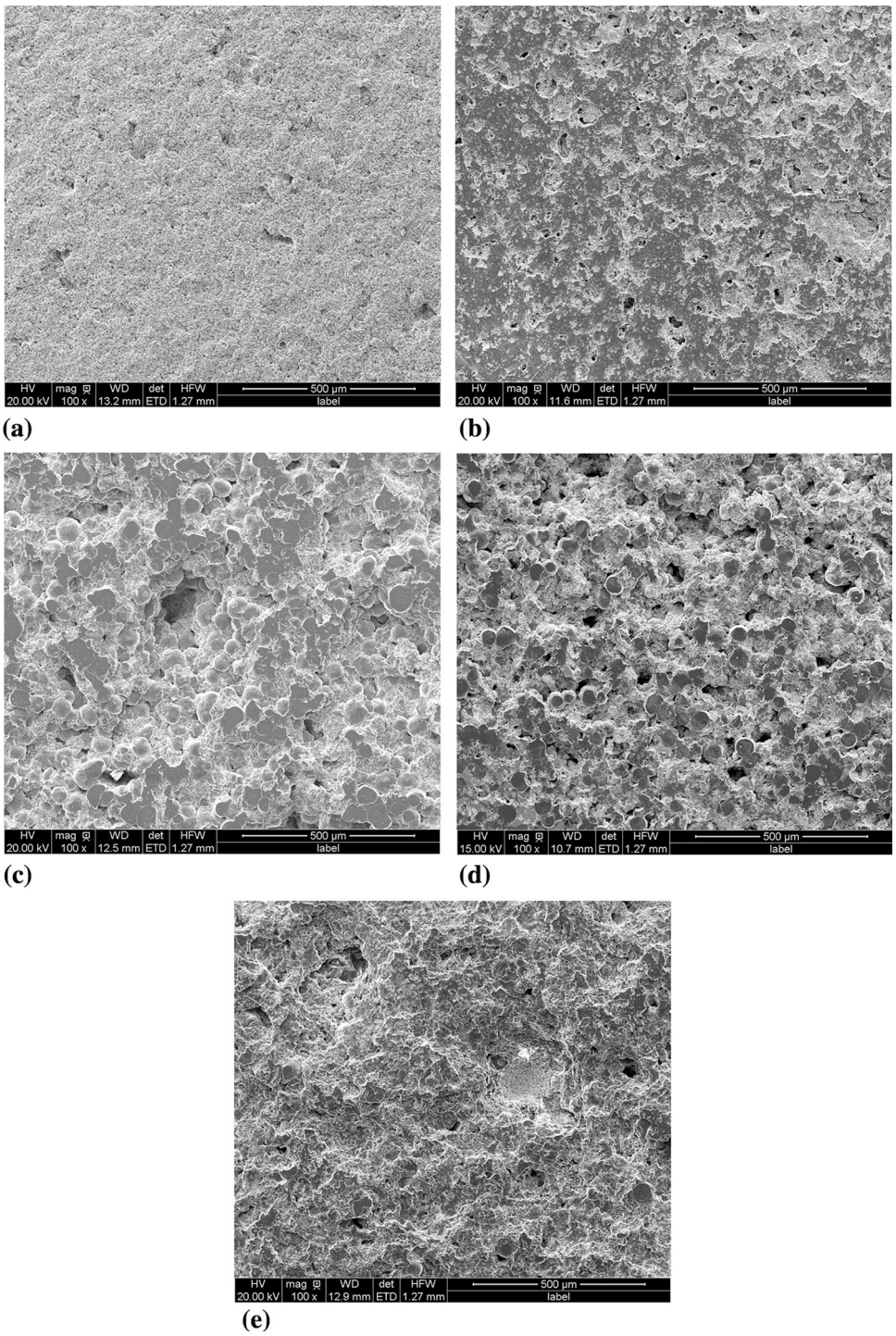

Fig. 9 FESEM morphologies of the surfaces of (a) 316L stainless steel, (b) WC-10Co4Cr coating, (c) Co-based coating, (d) WC-10Co4Cr/Co-based composite coating, and (e) Fe-based coating after cavitation exposure of 15 h in artificial seawater

was more readily eroded and material was removed by reason of the porosity and weaker bonding strength with other particles (Fig. 8d). Large cavitation craters were present at the boundary of different phases and several pinholes and comparatively small cavitation craters were present at or in close proximity to the surrounding of WC grains. The eroded surface of the Fe-based coating was the most seriously damaged coating when compared to the other four coatings (see Fig. 8e). Relatively large cavitation pits were present on the surface of the Fe-based coating and were mainly induced by cracks and the large pores that were already present as original defects. It can be inferred that the large cavitation craters produced by the impact energy propagated along the interfaces of the spray-coating layers because of their typical lamellar microstructure. Compared with the scars on the eroded

surfaces of the samples that were tested in deionized water, more serious damage was observed in the coatings that were tested in artificial seawater (Fig. 9). This may be because of the inferior corrosion resistance of the coating materials in an environment that contains chloride ions. This was a point that was made by Neville et al. (Ref 23) in relation to corrosion of WC-based overlays. The result is consistent with the cumulative volume loss data collected from tests that were conducted in deionized water and in artificial seawater (Fig. 6). However, it also should be noted that further comprehensive studies on the effect of marine corrosion on cavitation erosion of thermally sprayed coatings are required. Ongoing research efforts are required to predict the effect of the coatings on propeller lifetimes by conducting measurements and observations of the propellers under full-scale operation. Nevertheless, the present study here has shed light on the potential cavitation-resistant applications of HVOF-sprayed WC-10Co4Cr coatings for marine vehicles and devices.

Conclusions

The cavitation erosion behaviors of HVOF-sprayed WC-10Co4Cr coatings, Co-based coatings, WC-10Co4Cr/Co-based composite coatings, and Fe-based amorphous/nanocrystalline coatings, as well as 316 L stainless steel substrates were studied and compared for testing in deionized water and in artificial seawater. This enabled an exploration of the effect of marine corrosion on the cavitation erosion behavior of coatings-based materials. The influence of seawater corrosion on cavitation erosion was most significant in stainless steel, WC-10Co4Cr coatings, and Co-based coatings, but negligible in WC-10Co4Cr/Co-based composite coatings and Fe-based amorphous/nanocrystalline coatings. Further, among the tested coating systems in both liquid media, the WC-10Co4Cr coatings provided the best cavitation erosion protection and can thus be suggested as a potential coating material for marine applications.

Acknowledgments This work was supported by China Scholarship Council (No. 201804910094), CAS-Iranian Vice Presidency for Science and Technology Joint Research Project (Grant # 174433KYSB20160085), National Natural Science Foundation of China (Grants # 41706076, 31500772 and 21705158), Key Research and Development Program of Zhejiang Province (Grant # 2017C01003), International Scientific and Technological Cooperation Project of Ningbo (Grant # 2017D10011), and a Natural Sciences and Engineering Research Council of Canada Discovery Grant (Grant # NSERC RGPIN-2018-04298).

References

1. X. Ding, X.D. Cheng, C.Q. Yuan, J. Shi, and Z.X. Ding, Structure of Micro-nano WC-10Co4Cr Coating and Cavitation Erosion Resistance in NaCl Solution, *Chin. J. Mech. Eng.*, 2017, **30**(5), p 1239-1247
2. Z. Shi, J. Wang, Z. Wang, Y.T. Xiong, and Y. Zheng, Cavitation Erosion and Jet Impingement Erosion Behavior of the NiTi Coating Produced by Air Plasma Spraying, *Coatings*, 2018, **8**(10), p 346
3. S. Zhang, S. Wang, C.L. Wu, C.H. Zhang, M. Guan, and J.Z. Tan, Cavitation Erosion and Erosion-corrosion Resistance of Austenitic Stainless Steel by Plasma Transferred Arc Welding, *Eng. Fail. Anal.*, 2017, **76**, p 115-124
4. Q. Wang, S. Bai, and Z.D. Liu, Study on Cavitation Erosion-Corrosion Behavior of Mild Steel Under Synergistic Vibration Generated by Ultrasonic Excitation, *Tri. Trans.*, 2014, **57**, p 603-612
5. G. Hou, X. Zhao, H. Zhou, J. Lu, Y. An, J. Chen, and J. Yang, Cavitation Erosion of Several Oxy-fuel Sprayed Coatings Tested in Deionized Water and Artificial Seawater, *Wear*, 2014, **311**(1-2), p 81-92
6. J. Lin, Z. Wang, P. Lin, J. Cheng, X. Zhang, and S. Hong, Microstructure and Cavitation Erosion Behavior of FeNiCrB-SiNbW Coating Prepared by Twin Wires Arc Spraying Process, *Surf. Coat. Technol.*, 2014, **240**, p 432-436
7. W. Deng, Y. An, G. Hou, S. Li, H. Zhou, and J. Chen, Effect of Substrate Preheating Treatment on the Microstructure and Ultrasonic Cavitation Erosion Behavior of Plasma-Sprayed YSZ Coatings, *Ultrason. Sonochem.*, 2018, **46**, p 1-9
8. C.L. Wu, S. Zhang, C.H. Zhang, H. Zhang, and S.Y. Dong, Phase Evolution and Cavitation Erosion-corrosion Behavior of $FeCoCrAlNiTi_x$ High Entropy Alloy Coatings on 304 Stainless Steel by Laser Surface Alloying, *J. Alloys Compd.*, 2017, **698**, p 761-770
9. S. Zhang, C.L. Wu, C.H. Zhang, M. Guan, and J.Z. Tan, Laser Surface Alloying of FeCoCrAlNi High-Entropy Alloy on 304 Stainless Steel to Enhance Corrosion and Cavitation Erosion Resistance, *Opt. Laser Technol.*, 2016, **84**, p 23-31
10. C.T. Kwok, H.C. Man, F.T. Cheng, and K.H. Lo, Developments in Laser-based Surface Engineering Processes: With Particular Reference to Protection Against Cavitation Erosion, *Surf. Coat. Technol.*, 2016, **291**, p 189-204
11. S. Hong, Y. Wu, J. Zhang, Y. Zheng, Y. Qin, and J. Lin, Ultrasonic Cavitation Erosion of High-Velocity Oxygen-Fuel (HVOF) Sprayed Near-Nanostructured WC-10Co-4Cr Coating in NaCl Solution, *Ultrason. Sonochem.*, 2015, **26**, p 87-92
12. G. Hou, Y. An, X. Zhao, H. Zhou, and J. Chen, Effect of Alumina Dispersion on Oxidation Behavior as well as Friction and Wear Behavior of HVOF-Sprayed CoCrAlYTaCSi Coating at Elevated Temperature Up to 1000 °C, *Acta Mater.*, 2015, **95**, p 164-175
13. D. Niebuhr, Cavitation Erosion Behavior of Ceramics in Aqueous Solutions, *Wear*, 2007, **263**(1-6), p 295-300
14. G. Taillon, F. Pougoum, S. Lavigne, L. Ton-That, R. Schulz, E. Bousser, S. Savoie, L. Martinu, and J.-E. Klemberg-Sapieha, Cavitation Erosion Mechanisms in Stainless Steels and in Composite Metal-Ceramic HVOF Coatings, *Wear*, 2016, **364**, p 201-210

15. A. Furusawa, K. Hine, Y. Hayashi, and H. Takizawa, Formation of Particle of Bismuth-indium Alloys and Particle Diameter by Ultrasonic Cavitation, *Ultrason. Sonochem.*, 2019, **50**, p 322-330
16. R. Zhang, Y. Ren, D. Yan, P. Guo, and L. Li, Synthesis of Hydrophobic Fluorinated Polyurethanes and Their properties of Resistance to Cavitation and Wear, *Prog. Org. Coat.*, 2017, **104**, p 11-19
17. S. Lavigne, F. Pougoum, S. Savoie, L. Martinu, J.E. Klemberg-Sapieha, and R. Schulz, Cavitation Erosion Behavior of HVOF CaviTec Coatings, *Wear*, 2017, **386-387**, p 90-98
18. C.R. Ciubotariu, E. Secosan, G. Marginean, D. Frunzaverde, and V.C. Campian, Experimental Study Regarding the Cavitation and Corrosion Resistance of Stellite 6 and Self-fluxing Remelted Coatings, *J. Mech. Eng.*, 2016, **62**(3), p 154-162
19. Z. Wang, X. Zhang, J. Cheng, J. Lin, and Z. Zhou, Cavitation Erosion Resistance of Fe-Based Amorphous/Nanocrystal Coatings Prepared by High-Velocity Arc Spraying, *J. Therm. Spray Technol.*, 2014, **23**(4), p 742-749
20. S. Hong, Y. Wu, J. Zhang, Y. Zheng, Y. Qin, and J. Lin, Effect of Ultrasonic Cavitation Erosion on Corrosion Behavior of High-Velocity Oxygen-Fuel (HVOF) Sprayed Near-Nanostructured WC-10Co-4Cr Coating, *Ultrason. Sonochem.*, 2015, **27**, p 374-378
21. K.R. Kumar, M. Kamaraj, S. Seetharamu, and S.A. Kumar, A Pragmatic Approach and Quantitative Assessment of Silt Erosion Characteristics of HVOF and HVAF Processed WC-CoCr Coatings and 16Cr5Ni Steel for Hydro Turbine Applications, *Mater. Des.*, 2017, **132**, p 79-95
22. R.K. Kumar, M. Kamaraj, S. Seetharamu, T. Pramod, and P. Sampathkumaran, Effect of Spray Particle Velocity on Cavitation Erosion Resistance Characteristics of HVOF and HVAF Processed 86WC-10Co4Cr Hydro Turbine Coatings, *J. Therm. Spray Technol.*, 2016, **25**(6), p 1217-1230
23. A. Neville, F. Reza, S. Chiovelli, and T. Revega, Assessing Metal Matrix Composites for Corrosion and Erosion-corrosion Applications in the Oils Sands Industry, *Corrosion*, 2006, **62**, p 657-675
24. N. Melendez and A. McDonald, Development of WC-Based Metal Matrix Composite Coatings Using Low-pressure Cold Gas Dynamic Spraying, *Surf. Coat. Technol.*, 2013, **214**, p 101-109
25. N. Melendez, V. Narulkar, G. Fisher, and A. McDonald, The Effect of Reinforcing Particles on the Wear Rate of Low-Pressure Cold-Sprayed WC-Based MMC Coatings, *Wear*, 2013, **306**, p 185-195
26. S. Hong, Y. Wu, J. Zhang, Y. Zheng, Y. Zheng, and J. Lin, Synergistic Effect of Ultrasonic Cavitation Erosion and Corrosion of WC-CoCr and FeCrSiBMn Coatings Prepared by HVOF Spraying, *Ultrason. Sonochem.*, 2016, **31**, p 563-569
27. "Standard Practice for the Preparation of Substitute Ocean Water," D1141-98, *ASTM,* 2003
28. "Standard Test Method for Cavitation Erosion Using Vibratory Apparatus," G32-16, *ASTM,* 2016
29. D.A. Stewart, P.H. Shipway, and D.G. McCartney, Microstructural Evolution in Thermally Sprayed WC-Co Coatings: Comparison Between Nanocomposite and Conventional Starting Powders, *Acta Mater.*, 2000, **48**(7), p 1593-1604
30. D. Li, X. Chen, X. Hui, J. Wang, P. Jin, and H. Li, Effect of Amorphicity of HVOF Sprayed Fe-Based Coatings on Their Corrosion Performances and Contacting Osteoblast Behavior, *Surf. Coat. Technol.*, 2017, **310**, p 207-213
31. H. Zhang, Y. Gong, B. Zhang, X. Chen, L. Fang, P. Jin, and H. Li, Corrosion and Algal Adhesion Behaviors of HVOF-Sprayed Fe-Based Amorphous Coatings for Marine Applications, *J. Therm. Spray Technol.*, 2019, **28**(1-2), p 283-290
32. W. Deng, G. Hou, S. Li, J. Han, X. Zhao, X. Liu, Y. An, H. Zhou, and J. Chen, A New Methodology to Prepare Ceramic-Organic Composite Coatings with Good Cavitation Erosion Resistance, *Ultrason. Sonochem.*, 2018, **44**, p 115-119
33. A. Krella and A. Czyzniewski, Influence of the Substrate Hardness on the Cavitation Erosion Resistance of TiN Coating, *Wear*, 2007, **263**(1-6), p 395-401
34. L. Qiao, Y. Wu, S. Hong, J. Zhang, W. Shi, and Y. Zheng, Relationships Between Spray Parameters, Microstructures and Ultrasonic Cavitation Erosion Behavior of HVOF Sprayed Fe-based Amorphous/Nanocrystalline Coatings, *Ultrason. Sonochem.*, 2017, **39**, p 39-46
35. A. Ayyagari, V. Hasannaeimi, H.S. Grewal, H. Arora, and S. Mukherjee, Corrosion, Erosion and Wear Behavior of Complex Concentrated Alloys: A Review, *Metals*, 2018, **8**(8), p 603
36. H. Liu, T. Zhang, and C. Kang, Evaluation of Cavitation Erosion Resistance of Copper Alloy in Different Liquid Media, *Mater. Corros.*, 2018, **69**, p 917-925
37. Q. Luo, Q. Zhang, Z. Qin, Z. Wu, B. Shen, L. Liu, and W. Hu, The Synergistic Effect of Cavitation Erosion and Corrosion of Nickel-aluminum Copper Surface Layer on Nickel-aluminum Bronze Alloy, *J. Alloys Compd.*, 2018, **747**, p 861-868
38. M.A. Islam and Z. Farhat, Erosion-corrosion Mechanism and Comparison of Erosion-Corrosion Performance of API, Steels, *Wear*, 2017, **376-377**, p 533-541
39. J. Ryl, J. Wysocka, P. Slepski, and K. Darowicki, Instantaneous Impedance Monitoring of Synergistic Effect Between Cavitation Erosion and Corrosion Processes, *Electrochim. Acta*, 2016, **203**, p 388-395
40. E. Sadeghimeresht, N. Markocsan, and P. Nylén, A Comparative Study of Corrosion Resistance for HVAF-Sprayed Fe- and Co-Based Coatings, *Coatings*, 2016, **6**(2), p 16
41. M.M. Lima, C. Godoy, P.J. Modenesi, J.C. Avelar-Batista, A. Davison, and A. Matthews, Coating Fracture Toughness Determined by Vickers Indentation: An Important Parameter in Cavitation Erosion Resistance of WC-Co Thermally Sprayed Coatings, *Surf. Coat. Technol.*, 2004, **177-178**, p 489-496
42. L.A. Espitia and A. Toro, Cavitation Resistance, Microstructure and Surface Topography of Materials Used for Hydraulic Components, *Tribol. Int.*, 2010, **43**, p 2037-2045